Dual-Bandstop Substrate-Integrated-Coaxial Tunable and Static RF Filters

Dimitra Psychogiou, *Senior Member, IEEE*, Kunchen Zhao, *Student Member, IEEE*, and Roberto Gómez-García, *Senior Member, IEEE*

***Abstract*— This letter discusses the RF design and practical realization of dual-bandstop filters (BSFs) with compact size and two independently controlled rejection bands. They are based on miniaturized substrate-integrated-coaxial (SIC) resonant stages that are made from two capacitively loaded posts and a thru-line. Each of the stages creates two transmission zeros (TZs) that can be exploited for the realization of dual-bandstop RF filters with approximately half the size of conventional single-post series-cascaded SIC filter configurations. Further miniaturization is achieved by tuning the center frequency of the bands. For proof-of-concept validation purposes, three prototypes were designed, manufactured, and measured. They include a static (rejection bands centered at 4 and 4.5 GHz) and a tunable (between 3.6–4.6 GHz) dual-bandstop second-order RF filters and a third-order dual-bandstop RF filter with bands centered at 4 and 4.4 GHz.**

***Index Terms*— Bandstop filter (BSF), coaxial filter, compact filter.**

I. Introduction

MICROWAVE bandstop filters (BSFs) are fundamental counterparts of ultrawideband communications and radar systems that need to acquire broad parts of the RF spectrum in the presence of interference [1]. More recently, tunable and multi-notch BSFs are also being sought for interference-resilient sub-6-GHz wireless communications due to the large number of co-existing applications [2], [3]. A wealth of planar BSFs have been presented to date. They exhibit multiple rejection bands (e.g., 1–3 in [3] and [4]) and wide center-frequency (f_{cen}) tuning. Multi-functional BSFs with embedded notches within reconfigurable passbands have also been reported [3], [4]. Despite their high levels of versatility, the rejection levels (20–40 dB) of planar BSFs are limited by the low-quality factor (Q) of their resonators—about 12–80.

Three-dimensional (3-D) BSFs, such as those based on substrate-integrated-coaxial (SIC) [5]–[9] and substrate-integrated-waveguide (SIW) [10]–[14] architectures, enable significantly higher Qs (100–600) and isolation (IS). In particular, SIC-based BSFs exhibit among the smallest physical size and widest tuning range—i.e., one octave of f_{cen} tuning with >40 dB of IS [7], [9]. Nevertheless, they are only able to suppress a single band, except for the dual-bandstop BSF in [10]. Dual-band BSF configurations using SIWs have also been shown [11]–[14]. However, they are static and larger than their SIC counterparts.

Considering the aforementioned limitations, this letter presents the design and practical development of ultra-compact and tunable dual-bandstop SIC BSFs. The proposed filter concept exhibits significantly smaller size (reduced by about 50%) than that of a conventional dual-band BSF in which two rejection bands are created by cascading two single-post SIC BSFs (e.g., as in [6]). The content of this letter is organized as follows. Section II discusses the operating principles of the dual-bandstop stage and its application to high-order transfer functions. In Section III, the concept is validated through the testing of two prototypes. RF tuning is also discussed. Finally, the contributions of this work are outlined in Section IV.

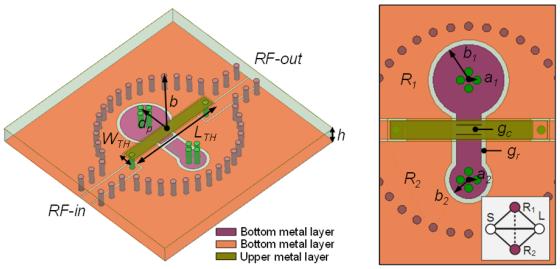

Fig. 1. Three-dimensional simulation model of the dual-bandstop SIC resonant stage that comprises two capacitively loaded posts and a thru-line. Left: bird-eye view. Right: top view. A block diagram of its corresponding coupling routing diagram comprising two resonating nodes (brown), two non-resonating nodes (white), and coupling elements (black lines) is also shown. The geometrical dimensions are: $b = 12$ mm, $d_p = 6$ mm, $W_{TH} = 2.2$ mm, $L_{TH} = 19.5$ mm, $b_1 = 4.3$ mm, $a_1 = 1.5$ mm, $b_2 = 2.3$ mm, $a_2 = 1.5$ mm, $g_r = 0.6$ mm, $g_c = 1$ mm, and $h = 3.175$ mm.

II. Theoretical Foundations

The details of the dual-bandstop SIC resonant stage are shown in Fig. 1. It comprises a dielectric-filled cylindrical cavity and two capacitively loaded metallic posts and it can be viewed as an SIC resonator with two electromagnetically (EM) coupled coaxial posts. The posts and the outer walls of the cavity are shaped by Cu-metallized via holes. For a bandstop response, the RF signal is inserted through an inverted coplanar-waveguide (CPW) transmission line (TL). For fixed cavity dimensions, f_{cen} of each band is controlled by the size of each post. For example, lower f_{cen} can be achieved for posts with smaller capacitive gaps g_r or larger radius of

Manuscript received June 27, 2021; accepted July 16, 2021. Date of publication July 20, 2021; date of current version December 6, 2021. *(Corresponding author: Dimitra Psychogiou.)*

Dimitra Psychogiou was with the Department of Electrical, Computer, and Energy Engineering, University of Colorado at Boulder, Boulder, CO 80309 USA. She is now with the School of Engineering, University College Cork, Cork, T12 K8AF Ireland, and also with the Tyndall National Institute, Cork, T12 R5CP Ireland (e-mail: DPsychogiou@ucc.ie).

Kunchen Zhao is with the Department of Electrical, Computer, and Energy Engineering, University of Colorado at Boulder, Boulder, CO 80309 USA (e-mail: kunchen.zhao@colorado.edu).

Roberto Gómez-García is with the Department of Signal Theory and Communications, University of Alcalá, Alcalá de Henares, 28871 Madrid, Spain (e-mail: roberto.gomez.garcia@ieee.org).

Color versions of one or more figures in this letter are available at https://doi.org/10.1109/LMWC.2021.3098480.

Digital Object Identifier 10.1109/LMWC.2021.3098480

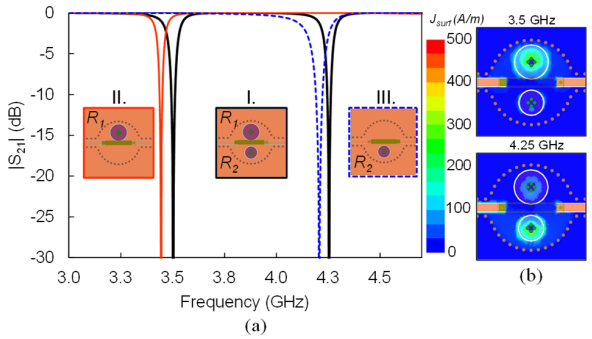

Fig. 2. (a) $|S_{21}|$ of the dual-bandstop stage (Example I: $b_1 = 4.8$ mm, $b_2 = 3.5$ mm) and two single-post SIC resonators each shaped by a post having the same size (e.g., $b_1 = 4.3$ mm in Example II and $b_2 = 3.5$ mm in Example III) as either of the posts in the dual-bandstop stage. (b) Magnitude of the current density on the bottom metal layer of the dual-bandstop SIC.

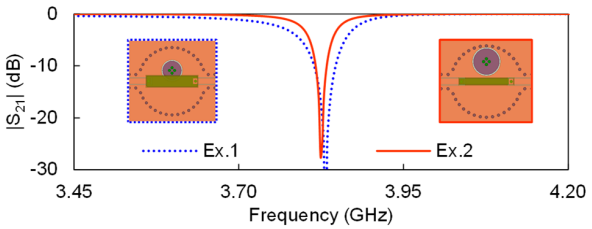

Fig. 3. Simulated $|S_{21}|$ as a function of W_{TH}, d_p, and b_1. Example 1: $W_{TH} = 4$ mm, $d_p = 4$ mm, and $b_1 = 3.5$ mm. Example 2: $W_{TH} = 2.2$ mm, $d_p = 7$ mm, and $b_1 = 4.55$ mm. The rest of the dimensions are listed in Fig. 1.

their upper disk (b_1 or b_2). The coupling between the posts can be modified by the distance of the posts d_P or the capacitive gap between the post disks g_c. d_p also alters the coupling of each post to the RF ports as shown in the coupling diagram in Fig. 1.

To demonstrate the operating principles of the concept, an example dual-band response is illustrated in Fig. 2(a) alongside the EM-simulated responses of two single-post SIC resonators (Examples II and III). Each of these resonators has the same cavity size as the dual-bandstop resonant stage and their posts are respectively assigned to have the same dimensions with R_1 and R_2. As shown in Fig. 2(a), the two rejection bands of the stage (Example I) appear at frequencies close to the ones of the single-post SIC resonators. The magnitude of the current density on the bottom metallization layer of the resonant stage is depicted in Fig. 2(b). As shown, the current is mostly higher around one of the two posts when excited by an RF signal at either of the rejection bands (e.g., at 3.5 or 4.25 GHz), indicating that each band is mostly controlled by one of the two posts. Thus, the dual-bandstop resonant stage can be readily designed by first specifying the dimensions of each of the single-post resonators using the method in [15] and by combining them afterward within a cavity that has the same dimensions as the one of the single-post resonators.

Whereas f_{cen} of each band is controlled by the dimensions of each post (e.g., a_1, b_1) and g_c, their 3-dB bandwidth (BW) depends on the external coupling, i.e., the distance of the post d_p and the impedance of the thru-line—controlled by W_{TH}. This is illustrated in Fig. 3 for the simple case of a single post. As shown, wider BWs can be obtained for posts closer to the TL and lower characteristic impedances.

Fig. 4 shows the effect of inter-post coupling for dual-bandstop resonant stages without [Fig. 4(a)] and with [Fig. 4(b)] capacitive coupling and variable b_1. As shown

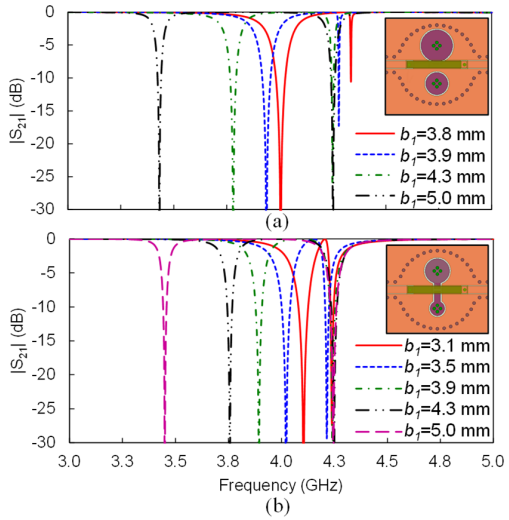

Fig. 4. $|S_{21}|$ of the dual-bandstop BSF SIC as a function of b_1. (a) Without coupling, $b_2 = 3.5$ mm. (b) With coupling, $b_2 = 2.3$ mm.

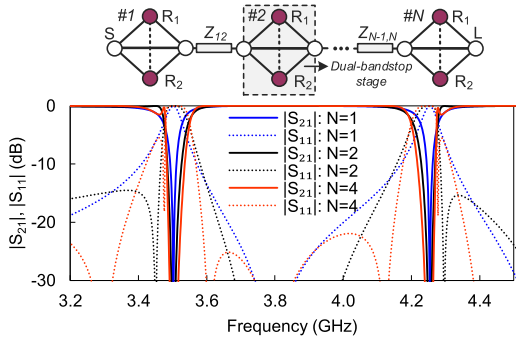

Fig. 5. Generalized block diagram of an N-stage dual-bandstop SIC BSF shaped by N stages and $N-1$ inverters (90°-long TLs at the average frequency of the two rejection bands). Each band is shaped by N TZs and EM-simulated S-parameters of a one-, a two-, and a four-stage dual-bandstop SIC BSFs. The impedance of the interconnecting inverters is around 50 Ω.

in Fig. 4(a), smaller values of b_1 bring the lower band closer to the high-frequency one. However, f_{cen} and BW of the high-frequency band are significantly altered when the bands get close to each other due to the change in the EM fields within the shared cavity when the dimensions of one of the posts are altered, thus affecting the coupling to the second post. On the contrary, when the capacitive coupling between the upper disks is present [see Fig. 4(b)] it dominates the overall coupling between the two posts, which is less influenced by the changes in the disk dimensions. As such, the resonant stage can be designed for both closely and widely spaced bands. This is really important for the design of tunable BSFs whose bands need to be independently tuned to closely and widely spaced bands. Having determined the characteristics of the resonant stage, higher order transfer functions can be realized by cascading multiple stages with 90°-long (defined at the average frequency of the two bands) TLs. This is shown in Fig. 5 for three different transfer function examples for dual-band BSFs comprising one, two, and four stages.

III. Experimental Validation

For proof-of-concept validation purposes, three filter prototypes were designed and tested. They include: 1) a static second-order; 2) a tunable second-order; and 3) a static third-order and they were designed in HFSS using the guidelines in Section II. They were built on a Rogers TMM

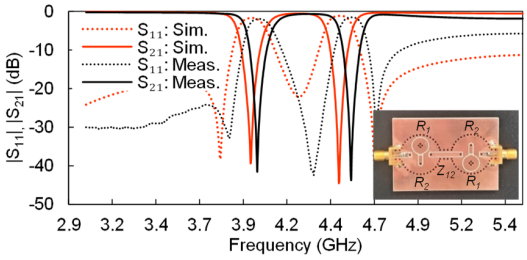

Fig. 6. Manufactured prototype, RF-measured, and EM-simulated S-parameters of the static dual-bandstop BSF prototype.

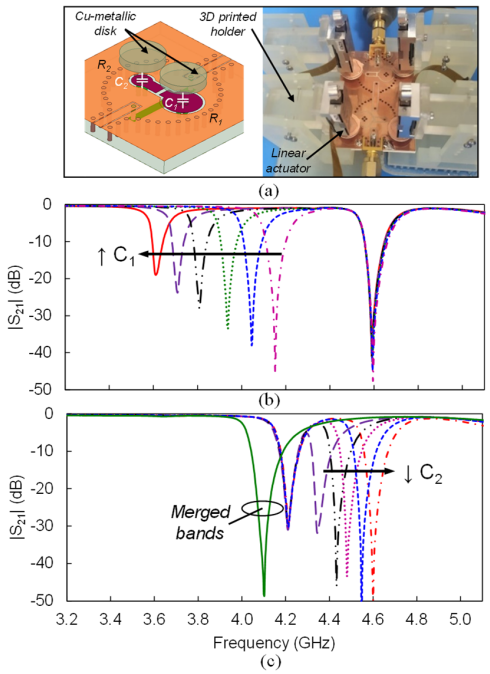

Fig. 7. (a) Tuning concept and manufactured prototype of the tunable dual-bandstop SIC BSF. RF-measured $|S_{21}|$. (b) Tuning of the lower frequency band while the upper band is fixed at 4.6 GHz. (c) Tuning of the upper frequency band while the lower band is fixed at 4.2 GHz and band merging.

3 substrate ($h = 3.175$ mm, dielectric constant: 3.27 and dissipation factor: 0.002) and they were tested with a Keysight N5224A PNA. The manufactured prototype and measured S-parameters of the static second-order prototype are shown in Fig. 6. It exhibits the following characteristics: 1) lower band: f_{cen}: 4 GHz, IS at f_{cen}: 41.5 dB, BW: 177 MHz (4.4%) and 2) upper band: f_{cen}: 4.51 GHz, IS at f_{cen}: 44 dB, BW: 160 MHz (3.5%). A comparison with its EM-simulated response is also shown in Fig. 6 validating the proposed dual-bandstop BSF concept. The frequency shift between EM simulations and measurements is fairly small (<1%) and mostly attributed to manufacturing tolerances.

To evaluate the tunability of the dual-bandstop SIC BSF, a reconfigurable prototype was manufactured and tested. The tuning concept and characterization setup are shown in Fig. 7(a). f_{cen} of each band is tuned by altering the capacitance between the post and a metal plate (placed on top of the post), as shown in Fig. 7(a). For validation, the tuner was implemented by a Cu-plated dielectric disk that was attached at the bottom of commercially available linear actuator from New Scale Tech. with maximum linear motion of 6 mm and 0.5 μm of resolution [16]. To enable their integration, a fixture was 3-D-printed. The RF-measured performance of the filter is provided in Fig. 7(b) and (c). Fig. 7(b) shows how the lower band can be tuned independently by only altering

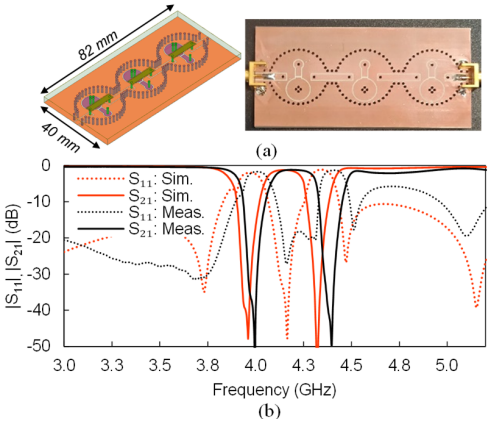

Fig. 8. (a) Manufactured prototype and EM model of the third-order prototype. (b) RF-measured and EM-simulated S-parameters of the filter prototype in (a).

TABLE I
COMPARISON WITH STATE-OF-THE-ART SIC/SIW BSFS

Ref.	[11]	[12]	[13]	[10]	[14]	T.W
Tech.	SIW	SIW	SIW	Coax	SIW	Coax
Size (cm^2)	30	59	N/A	N/A	10	22/32
Size (λ_0^2)	4.9	3.2	N/A	N/A	0.03	0.41/0.6
N	3	3	1, 2	2	2	2/3
SB	2	2	2	2	2	2
f_{cen} (GHz)	11.6, 12.6 static	6.8, 7.2 static	3.5-4.1, 5.6	3-3.5, 3.1-3.7	1.4-1.6, 1.7-1.9	3.6-4.2,4.3-4.6/4,4.4
IS (dB)	38, 21	60, 60	13, 13	25-40	22-28	20-46/64,51

N: order, SB: Stopbands, IS: Isolation, N/A: Not available, λ_0: free-space wavelength at the average frequency of the tuning range.

the capacitance of R1. Similarly, independent tuning of the upper frequency band is shown in Fig. 7(c). Furthermore, the bands can be merged to a single band allowing to control the number of rejection bands. Although a finite number of states are provided, the filter can be tuned continuously within the 3.6–4.6-GHz range. To explore scalability to higher order transfer functions, a third-order architecture was designed and tested. Its RF performance is illustrated in Fig. 8 and is summarized as follows: 1) lower band: f_{cen}: 4 GHz, IS at f_{cen}: 64 dB, BW: 185 MHz (4.6%) and 2) upper band: f_{cen}: 4.4 GHz, IS at f_{cen}: 51 dB, BW: 167 MHz (3.8%). A comparison with the EM-simulated response is also provided and it appears to be in good agreement. Furthermore, the SIC dual-bandstop BSF concept is compared with the state-of-the-art (SOA) 3-D SIC/SIW BSFs in Table I. As shown, this is the only configuration that allows for wide tuning and independent control of both its bands alongside band merging. Moreover, it can be designed for both widely and closely spaced bands. Finally, the proposed filter concept is smaller than most of the filters in Table I and about 50% smaller than a conventional SIC BSF approach.

IV. CONCLUSION

Static and tunable dual-bandstop SIC BSFs have been presented in terms of design and experimental validation. The proposed filter concept allows for dual-bandstop RF filters with significantly smaller size than the SOA, as well as realization of both closely and widely spaced rejection bands. RF tuning using commercially available actuators has also been shown, demonstrating the potential to independently tune the rejection bands within a wide range of frequencies.

REFERENCES

[1] W. J. Chappell, E. J. Naglich, C. Maxey, and A. C. Guyette, "Putting the radio in 'software-defined radio': Hardware developments for adaptable RF systems," *Proc. IEEE*, vol. 102, no. 3, pp. 307–320, Mar. 2014.

[2] Y. Sun, B. Chi, and H. Zhang, "Guest editorial for the special issue on software-defined radio transceivers and circuits for 5G wireless communications," *IEEE Trans. Circuits Syst. II, Exp. Briefs*, vol. 63, no. 1, pp. 1–3, Jan. 2016.

[3] D. Psychogiou, R. Gómez-García, and D. Peroulis, "Fully adaptive multiband bandstop filtering sections and their application to multifunctional components," *IEEE Trans. Microw. Theory Techn.*, vol. 64, no. 12, pp. 4405–4418, Dec. 2016.

[4] D. Psychogiou, R. Gómez-García, and D. Peroulis, "RF wide-band bandpass filter with dynamic in-band multi-interference suppression capability," *IEEE Trans. Circuits Syst. II, Exp. Briefs*, vol. 65, no. 7, pp. 898–902, Jul. 2018.

[5] E. J. Naglich, J. Lee, D. Peroulis, and W. J. Chappell, "Extended pass-band bandstop filter cascade with continuous 0.85–6.6-GHz coverage," *IEEE Trans. Microw. Theory Techn.*, vol. 60, no. 1, pp. 21–30, Jan. 2012.

[6] A. Anand and X. Liu, "Capacitively tuned electrical coupling for reconfigurable coaxial cavity bandstop filters," in *IEEE MTT-S Int. Microw. Symp. Dig.*, Phoenix, AZ, USA, May 2015, pp. 1–3.

[7] T. Snow, J. Lee, and W. J. Chappell, "Tunable high quality-factor absorptive bandstop filter design," in *IEEE MTT-S Int. Microw. Symp. Dig.*, Montreal, QC, Canada, Jun. 2012, pp. 1–3.

[8] M. D. Hickle and D. Peroulis, "Tunable constant-bandwidth substrate-integrated bandstop filters," *IEEE Trans. Microw. Theory Techn.*, vol. 66, no. 1, pp. 157–169, Jan. 2018.

[9] W. Yang, M. D. Hickle, D. Psychogiou, and D. Peroulis, "L-band high-Q tunable quasi-absorptive bandstop-to-all-pass filter," in *IEEE MTT-S Int. Microw. Symp. Dig.*, Honololu, HI, USA, Jun. 2017, pp. 271–273.

[10] K. Lee, T. H. Lee, C. S. Ahn, Y. S. Kim, and J. Lee, "Reconfigurable dual-stopband filters with reduced number of couplings between a transmission line and resonators," *IEEE Microw. Wireless Compon. Lett.*, vol. 25, no. 2, pp. 106–108, Feb. 2015.

[11] F. Yang, H.-X. Yu, X.-Y. He, Y. Zhou, and R.-Z. Liu, "Novel multi-band filter design and substrate integrated waveguide filter realization," in *IEEE MTT-S Int. Microw. Symp. Dig.*, Montreal, QC, Canada, Jun. 2012, pp. 1–3.

[12] F. Cheng, X.-T. Li, P. Lu, and K. Huang, "Synthesis and design of SIW dual-band narrow-band bandstop filter," *Electromagnetics*, vol. 40, no. 5, pp. 303–312, Jun. 2020.

[13] M. Esmaeili and J. Bornemann, "Novel tunable bandstop resonators in SIW technology and their application to a dual-bandstop filter with one tunable stopband," *IEEE Microw. Wireless Compon. Lett.*, vol. 27, no. 1, pp. 40–42, Jan. 2017.

[14] T. R. Jones and M. Daneshmand, "Miniaturized reconfigurable dual-band bandstop filter with independent stopband control using folded ridged quarter-mode substrate integrated waveguide," in *IEEE MTT-S Int. Microw. Symp. Dig.*, Boston, MA, USA, Jun. 2019, pp. 102–105.

[15] A. Anand, J. Small, D. Peroulis, and X. Liu, "Theory and design of octave tunable filters with lumped tuning elements," *IEEE Trans. Microw. Theory Techn.*, vol. 61, no. 12, pp. 4353–4364, Dec. 2013.

[16] New Scale Technologies. (2018). *M3-L Micro Linear Actuator With Embedded Controller*. [Online]. Available: https://www.newscaletech.com/micro-motion-modules/m3-l-linear-smart-actuators